Int. J. Electrochem. Sci., 15 **(2020)** 6207 – 6216, doi: 10.20964/2020.07.16

International Journal of
ELECTROCHEMICAL
SCIENCE
www.electrochemsci.org

Constructing Fe_3O_4/Nitrogen-doped Graphene Composites with Rich Pyrrolic Nitrogen for Excellent Supercapacitor Performance

Jugong Zheng, Ting Yang, Jianfa Chen, Jianping Xu[*]*, Tianxiang Jin*[*]

Jiangxi Engineering Research Center of Process and Equipment for New Energy, East China University of Technology, Nanchang 330013, P.R. China
[*]E-mail: 201660027@ecut.edu.cn (T. X. Jin), xujp@ecut.edu.cn (J. P. Xu)

Received: 1 March 2020 / *Accepted:* 17 April 2020 / *Published:* 10 June 2020

Nitrogen-doped graphene (NG)-supported Fe_3O_4 nanoparticle composites were prepared via a facile solvothermal and calcination process. The experimental results showed that the Fe_3O_4 nanoparticles were evenly embedded in the surface of NG without agglomeration and that pyrrolic N was the main N binding form in NG. The as-prepared Fe_3O_4@NG composites displayed a good specific capacitance of 244.3F/g at a current density of 1A/g. Furthermore, the Fe_3O_4/NG composites exhibited a low capacitance loss after 1000 cycles.

Keywords: Nitrogen-doped graphene, Fe_3O_4 nanoparticles, supercapacitor, electrode material

1. INTRODUCTION

Generally electrochemical methods are sensitive, stable, and accurate [1-3] and have been widely used in applications, such as electrochemical biosensors [4-6], supercapacitors [7], fuel cells [8, 9]. As one of the most indispensable energy storage devices, supercapacitors have many notable features such as multifunctionality, excellent cycle stability, and low cost. [10, 11] Nevertheless, the low energy density of supercapacitors limits their further application. Therefore, it is significant to find effective strategies for enhancing the energy density of supercapacitors without reducing their power density and cycle stability. [12, 13] Facts show that the electrode materials have a significant impact on the performance of supercapacitors. Many studies have been conducted on the use of transition metal oxides as electrode materials because of their large pseudocapacitance. [14, 15] However, pseudocapacitor materials have poor rate capacities and cyclic stabilities during charging and discharging; specifically, the cyclic stability is far less stable than that of the double layer capacitance. [15] Therefore, a hybrid material that is composed of carbon-based materials and metal oxides could be a high-performance electrode material because it has the advantages of integrating an electronic double-layer capacitor

(EDLC) and a pseudocapacitor. [16, 17] Many composites that involve the combination of metal oxides (such as Co_3O_4, [18] MnO_2, [19, 20] MoO_2, [21] V_2O_5, [22] SnO_2 [23]) and carbon-based materials generally exhibit excellent electrochemical energy storage performance. [24, 25]

Fe_3O_4 is an attractive material for pseudocapacitor electrodes, and has the advantages of a wide range for the operational potential window (−1.2 to 0.25V), low cost, large theoretical specific capacitance (2299F/g), and excellent conductivity (10^2-10^3S/cm). [26-28] The surface morphology, [29] crystallinity, [30] and particle distribution [31] of Fe_3O_4 largely influence the supercapacitive performance. Khoh synthesized multilayer films made of Fe_3O_4 nanoparticles and reduced graphene oxide (RGO) using a layer-by-layer progressive approach. The as-synthesized multilayer films exhibited excellent capacitive performances with 151 F/g at 0.9 A/g. [32] Meng synthesized porous Fe_3O_4/carbon composites via calcination of an iron-based metal organic framework. This material displayed a specific capacitance of 139 F/g at 0.5 A/g. [33] Ghasemi synthesized an RGO/Fe_3O_4 composite via a simple electrophoretic deposition and electrochemical reduction method. This nanocomposite displayed a specific capacitance of 154 F/g at 1 A/g. [34]

Although all the above composites have good energy storage properties, the synthesis methods of these composites are extremely sophisticated, and it is difficult to control the final microstructure of Fe_3O_4. It is known that metal oxide particles that have large specific surface area generally have a high specific capacitance. [35] However, magnetic nano-Fe_3O_4 particles have a tendency to agglomerate during the preparation process, and this leads to larger sized particles. [28] Therefore, if the specific surface area of Fe_3O_4 on the RGO surface can be increased, the material can, in theory, exhibit better electrochemical performance. [36]

Graphene is a new type of carbon material and has the characteristics of good conductivity and large specific surface area, which make it suitable for energy storage devices [37]. Moreover, graphene can also act as a support network for embedding Fe_3O_4 nanoparticles to prevent Fe_3O_4 from agglomerating. [28] However, graphene has low polarity, and it usually has poor interaction with metal oxides, and this is not conducive for the immobilization and dispersion of Fe_3O_4 magnetic nanoparticles. To solve the above problem, we attempted to introduce nitrogen atoms into the graphene lattice to enhance the interaction between graphene and Fe_3O_4. [38, 39]

Thus, we developed a simple hydrothermal and annealing approach for preparing Fe_3O_4/N-doped graphene (Fe_3O_4@NG) nanocomposites. We found that the pyrrolic N was the major sort of N in the NG that was synthesized via this method. Pyrrolic N has good electron-donor characteristics that can efficiently improve the electrochemical performance of electrode materials. Electrochemical testing was used to test the composites, and the as-obtained Fe_3O_4@NG composite-based supercapacitors exhibited excellent performance.

2. EXPERIMENTAL

2.1. Chemicals

$FeCl_3$•$6H_2O$, cetyltrimethylammonium bromide (CTAB), urea, and ethylene glycol (EG) were obtained from Sigma-Aldrich. KMnO4, KOH, NaNO3, 98% H2SO4, 30% H2O2, and graphite powder were obtained from China Medicine Co. All the reagents were of analytical grade.

2.2 Preparation of Fe_3O_4 @ NG composites

GO was synthesized from graphite powder via a modified improved Hummer method [40]. Ultrasonication was used for 30min to disperse GO in aqueous solution (2mg/mL, 50mL). Subsequently, 1.35g $FeCl_3 \cdot 6H_2O$, 0.5g CTAB, and 0.5mL EG were introduced in sequence and stirred for 0.5h. Then, 3g of urea that was dissolved in 25mL ethanol solution was added dropwise into the system, which was stirred for 0.5h. After that, the reaction solution was transferred into a 100mL Tefion-lined stainless steel autoclave that was maintained at 180℃ for 12h. After the autoclave was cooled to room temperature, the product was washed several times with DI water and anhydrous ethanol. Finally, the product was dried under vacuum at 80℃ for 24h. For comparison, NG was prepared without the added of $FeCl_3 \cdot 6H_2O$ using the same procedure. The synthetic route of the Fe_3O_4@NG composite is shown in Figure 1.

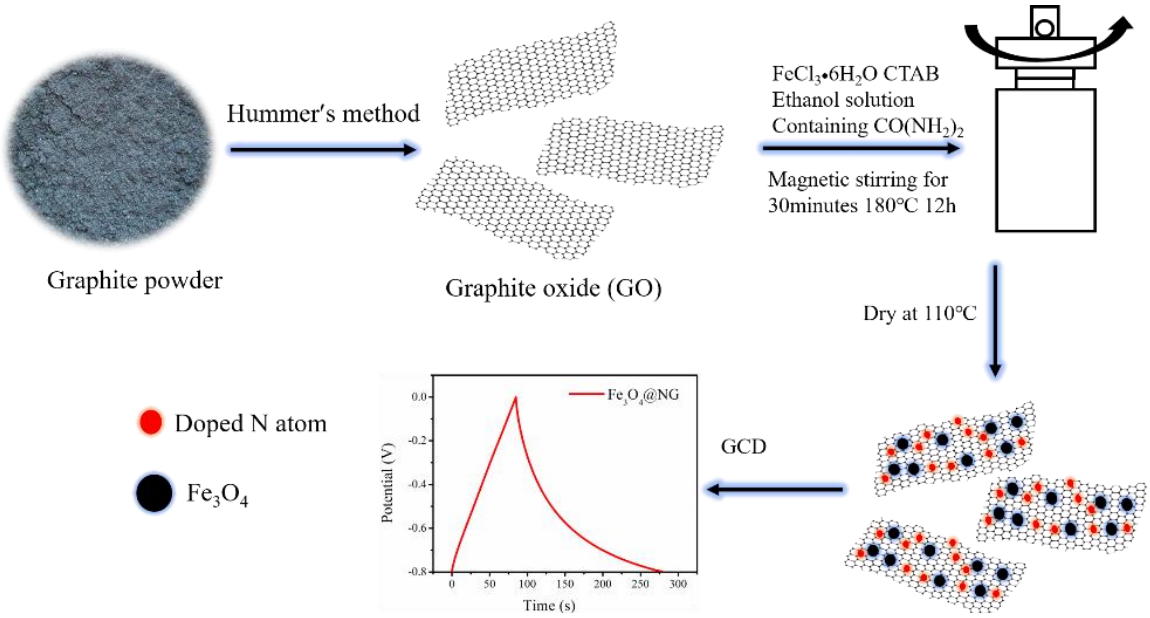

Figure 1. Schematic diagram of the synthesis process for Fe_3O_4@NG composites.

2.3 Characterization of materials

TEM observations were conducted using a JEM-2100F transmission electron microscope. XPS analyses were performed using a Thermo Fisher X-ray photoelectron spectrometer (Al Kα radiation).

2.4 Electrochemical Characterization

The working electrodes were fabricated using electroactive material, acetylene black, and polytetrafluoroethylene (PTFE) binder in a weight ratio of 80:15:5. These electrodes were pressed onto Ni-grids under a pressure of 15MPa. The area of the electrode was $1cm^2$. Electrochemical performances were assessed using cyclic voltammetry (CV) and galvanostatic charge-discharge (GCD) tests. All of the tests were conducted on a CHI 660E electrochemical cell equipped with a 3-electrode system in 1M

Na_2SO_4 solution at room temperature. The specific capacitance (Cs) was calculated from the GCD curves using equation (1).

$$Cs = \frac{I \cdot t}{m \cdot \Delta U} \qquad (1)$$

where I represents the discharge current, t is to the discharge time, m denotes the mass of the composites, and ΔV represents the voltage window.

3. RESULT AND DISCUSSION

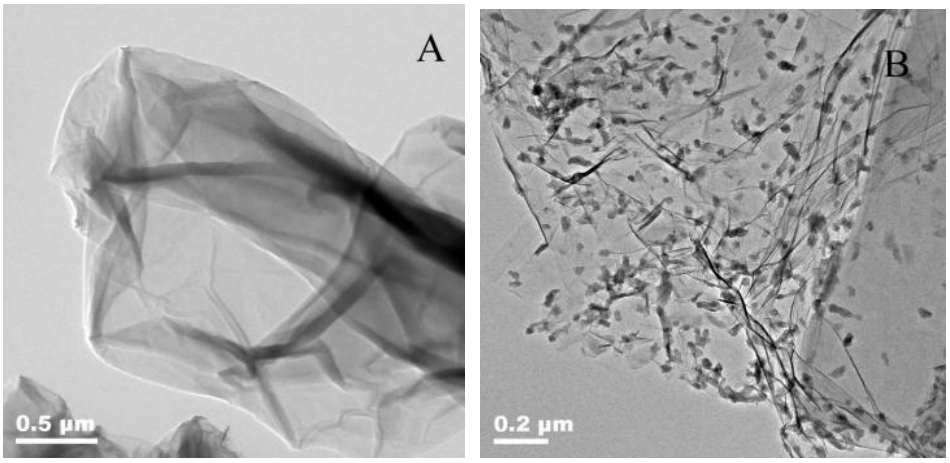

Figure 2. TEM images of (A) NG and (B) Fe_3O_4@NG.

The morphology of NG and Fe_3O_4@NG was assessed via TEM observations. As seen in Fig. 2A, NG exhibited a crumpled silk veil morphology. An image of as-prepared Fe_3O_4@NGs is displayed in Fig. 2B. Fe_3O_4 nanoparticles with a small size (of about 20 nm) were uniformly embedded in the surface of NG without agglomeration. This result may be attributed to the strong interaction between Fe_3O_4 and NG, which restrains the agglomeration of Fe_3O_4 nanoparticles.

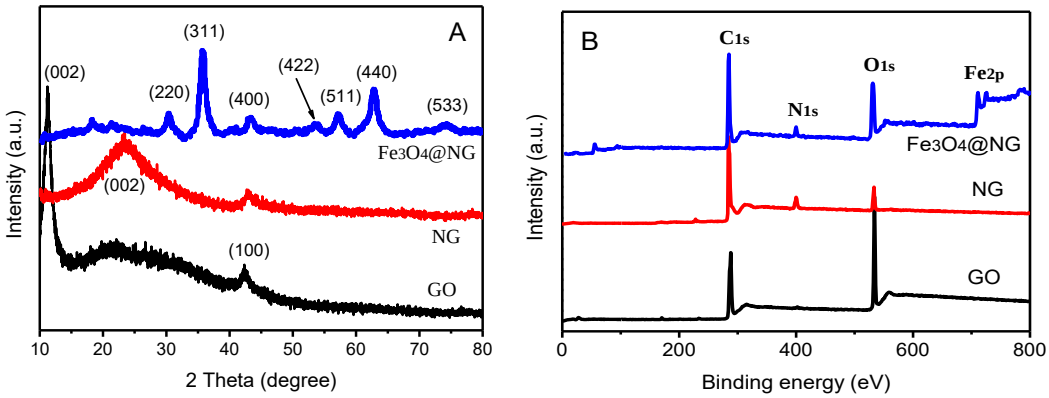

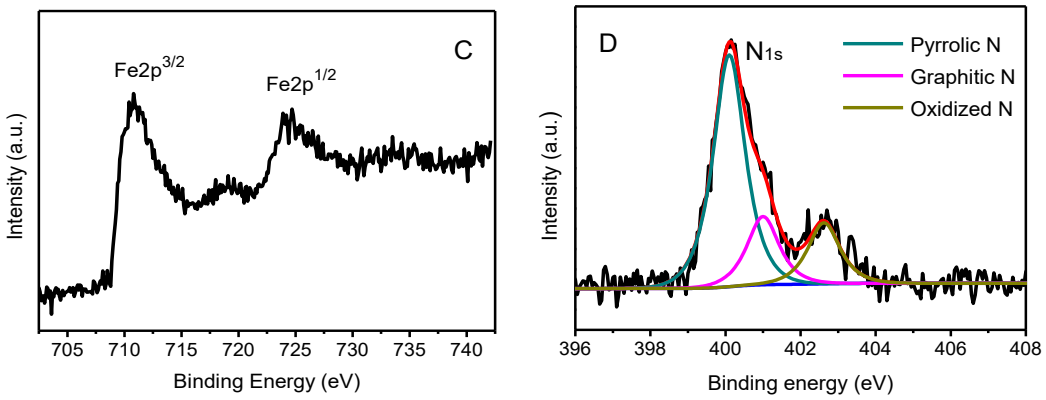

Figure 3. (A) XRD patterns and (B) XPS survey spectra of GO, NG, and Fe_3O_4@NG and high resolution XPS spectra of (C) Fe2p and (D) N1s.

Figure. 3A shows XRD patterns, and as seen, a sharp diffraction peak of GO appeared at 2θ = 11.2°, corresponding to the (002) crystal plane of carbon. This peak disappeared after reduction. Instead, a broad peak that corresponds to the (002) crystal plane of carbon appeared at 23.5° in NG, and this indicates poorly ordered graphene sheets. The diffraction peaks of Fe_3O_4@NG are at 2θ= 30.5°, 35.8°, 43.6°, 57.2°, 62.9°, and 73.9° and can be perfectly assigned to the diffraction planes (220), (311), (400), (422), (511) and (440), respectively. These results are in accord with the standard data (JCPDS no.19-0629). In particular, a sharp diffraction peak appeared at 35.8°, and this proves that Fe_3O_4 nanoparticles were loaded on the surface of NG and had a better crystal form without impurities.

X-ray photoelectron spectroscopy (XPS) was used to analyze the chemical composition of GO, NG, and Fe_3O_4@NG. As seen in Fig. 3B, C1s and O1s characteristic peaks appeared in the XPS spectrum of GO. After the nitrogen doping process, a new peak that corresponds to N1s appeared at a binding energy (BE) of 400 eV. The appearance of this peak confirms the successful incorporation of nitrogen into the carbon framework. Moreover, compared with the spectrum of GO, the O1s peak of NG at 532.2 eV was significantly weaker, and this indicates that GO was reduced during the doping process. Fig.2B also shows the characteristic peaks of the C 1s, N 1s, O 1s, and Fe 2p in the XPS spectra, proving that carbon, oxygen, nitrogen, and iron elements were present in the Fe_3O_4@NG composites. The results clearly indicate the successful incorporation of Fe_3O_4 nanoparticles into the carbon nanosheets. Compared with NG, Fe_3O_4@NG showed a significant increase in the O1s peak. These results are consistent with previous reports and further verify that Fe_3O_4 particles were successfully loaded on the surface of graphene. In the high resolution XPS Fe 2p spectrum (Fig.3C), there are two strong peaks at 711.8eV and 724.2 eV that correspond to Fe2p3/2 and Fe2p1/2 for Fe_3O_4. As seen in Fig.3D, the N1s peak can be deconvoluted into three components at 399.9 eV, 401.2 eV and 402.6 eV, which correspond to pyrrolic N, graphitic N, and oxidized N, respectively. Pyrrolic N is the dominant species in Fe_3O_4@NG composites. Pyrrolic N has a good electron donor property, and can effectively improve electrochemical performance. [41,42]

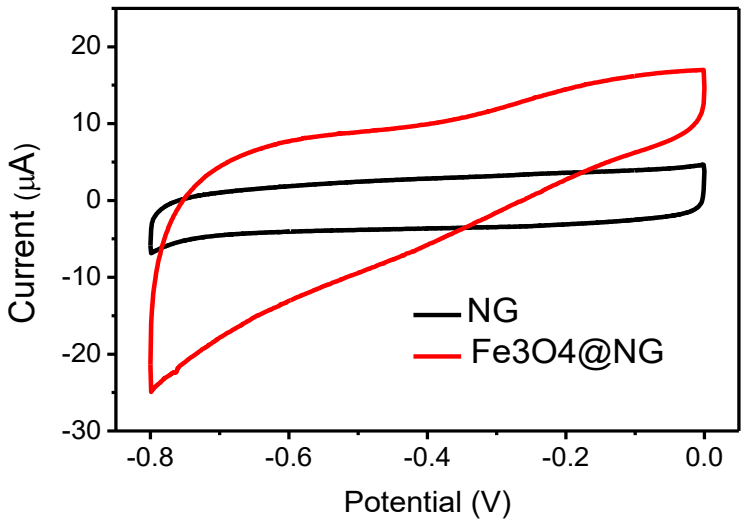

Figure 4. CV curves of NG and Fe_3O_4@NG composite modified electrodes at a scan rate of 20 m V/s in 1.0 M Na_2SO_4 solution.

CV curves of NG and Fe_3O_4@NG were recorded at a scan rate of 20mV/s at a three-electrode system with 1.0 M Na_2SO_4 as the electrolyte solution. As seen in Fig.4, the CV curve of Fe_3O_4@NG exhibited a near-rectangular shape with obvious redox peaks, and this indicates that the capacitance of Fe_3O_4@NG was the combination of the electric double-layer capacitance of NG and the Faraday pseudocapacitance from both NG and the Fe_3O_4 nanoparticles. It is known that the specific capacitance of an electrode is proportional to the area of the detected CV curve. Obviously, the enclosed area of the Fe_3O_4@NG composite was evidently larger than that of the NG electrode at the same scan rates, and this indicates that the Fe_3O_4@NG composite electrode has excellent capacitance.

GCD technology was used to further detect the capacitance performance of the NG electrode and the Fe_3O_4 @ NG composite electrode. GCD curves of the electrodes were recorded at a current density of 1 A/g within a potential range of -0.8–0 V. As seen in Fig.5, both the NG electrode and the Fe_3O_4@NG electrode displayed shapes that were quasi-isosceles triangles. The calculated specific capacitance of Fe_3O_4@NG is 244.3 F/g, which higher than that of NG (120.1 F/g). The larger specific capacitance of Fe_3O_4@NG is mainly attributed to the synergistic effect between Fe_3O_4 and NG. On one hand, NG provides a high specific surface area and enhances the dispersion of Fe_3O_4 nanoparticles. On the other hand, Fe_3O_4 can prevent agglomeration of NG. Because of this effect, both NG and the Fe_3O_4 nanoparticles had a large available surface; this can facilitate electron transport and promotes redox reactions across the electrode. [43] Also, the pyrrolic-N-rich structure of NG plays an important role in promoting the electrochemical performance.

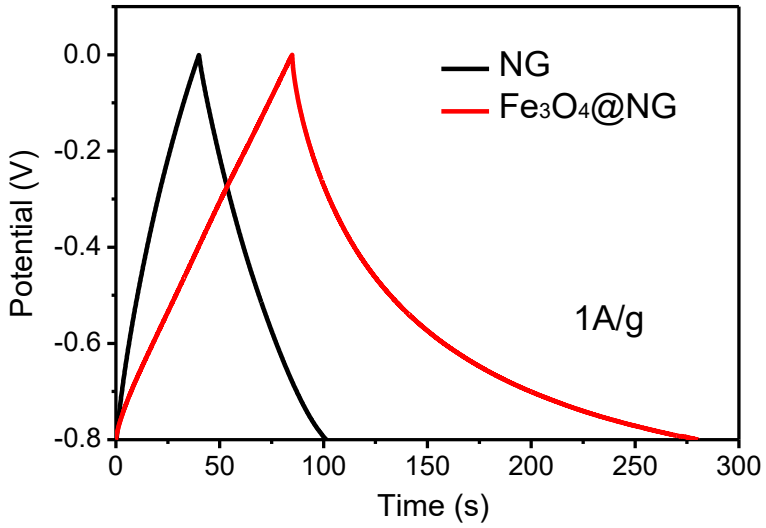

Figure 5. Constant current charge-discharge curves of NG and Fe_3O_4@NG

The specific capacitances of Fe_3O_4@NG under different current densities (1, 2, 3, 5, and 10 A/g) are shown in Fig. 6. The specific capacitances were calculated to be 244.3F /g, 198.7F /g, 182.5F /g, 168.8 F /g, and 161.2F /g at 1, 2, 3, 5,10 A/g, respectively. The corresponding specific capacitance retention rates are 100%, 81.33%, 74.70%, 69.09%, and 65.98%, respectively. These results prove that the Fe_3O_4@NG composites have good capacitance ratios at high current densities.

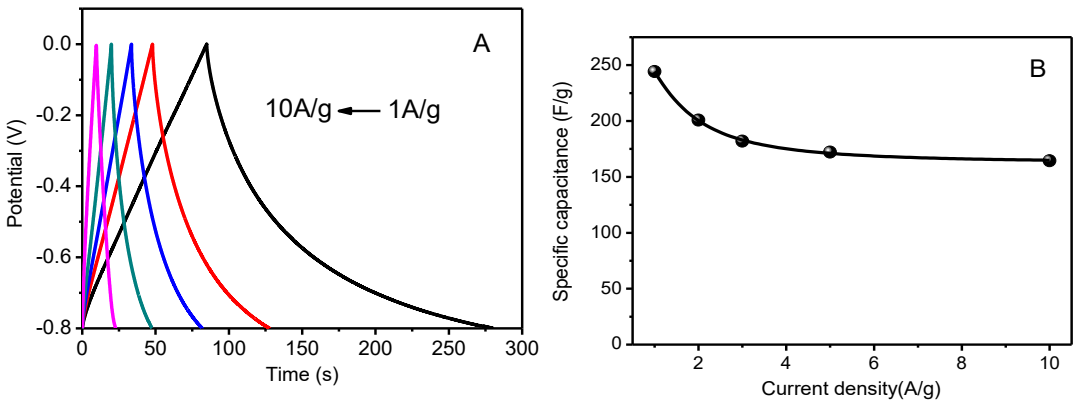

Figure 6. (A) Charge-discharge curves of the Fe_3O_4@NG electrode at current densities of 1, 2, 3, 5, and 10A/g. (B) Specific capacitance curves of Fe_3O_4@NG at different current densities.

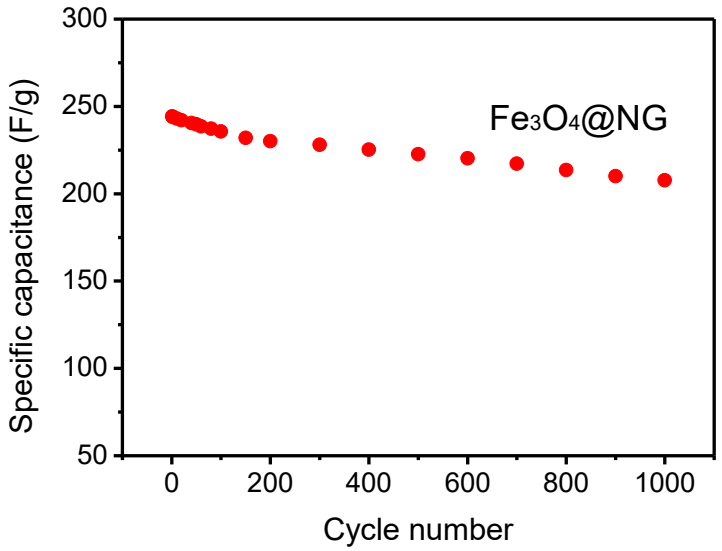

Figure 7. Changes in Cs for Fe_3O_4@NG composites with the number of cycles at a current density of 1 A/g.

The cycling stabilities of the NG and Fe_3O_4@NG electrodes were tested up to 1000 cycles, as displayed in Fig.7. The specific capacity of the Fe_3O_4@NG composite electrode decreased from an initial value of 244.3F/g to a value of 207.7F/g after 1000 cycles, and the specific capacitance still remained 85.02% of the initial capacity. These results prove that Fe_3O_4@NG has an advantageous long-term electrochemical stability. This excellent performance may be attributed to the strong interaction between nitrogen-doped graphene and Fe_3O_4 nanoparticles, which inhibited the destruction of the microstructure during redox reaction.

Table 1. Comparison of specific capacitance of different Fe-based composite electrode materials

Electrode Materials	Electrolyte	Cs(F/g)
CNT/Fe_3O_4 [44]	6 M KOH	117.2
Fe_3O_4/rGO [45]	1 M KOH	220.1
Fe_2O_3-5wt%CNT [46]	2 M KCl	54
Fe_3O_4/carbon nanosheets [47]	1 M Na_2SO_4	163.4
Fe_3O_4/CNF [48]	1 M Na_2SO_4	127
Fe_3O_4/rGO [43]	1 M KOH	241
Fe_3O_4/carbon nanofiber [49]	3M KOH	225
Fe_3O_4@NG (This work)	1M Na_2SO_4	244.3

To evaluate the electrochemical performance of Fe_3O_4@NG, the specific capacitance measured in this work was compared with that of reported in several previous studies of Fe-based electrodes. As seen in Table 1, the Fe_3O_4@NG electrode showed a competitive electrochemical performance, and this means that the Fe_3O_4@NG is an ideal electrode material.

4. CONCLUSIONS

In summary, the Fe_3O_4@NG composite material that was rich in pyrrolic N was successfully synthesized via a hydrothermal and calcination route. Fe_3O_4 nanoparticles that had a large specific surface area were uniformly embedded in NG sheets. Benefiting from the pyrrolic-N-rich structure of NG and the synergetic effect between NG and Fe_3O_4, the Fe_3O_4@NG composite electrode showed a high specific capacity of 244.3F/g at a current density of 1 A/g. Furthermore, the specific capacitance still remained 85 % of the initial capacity after 1000 cycles. Therefore, we have determined that the Fe_3O_4@NG composite has good electrochemical performance and is an excellent material for high-performance supercapacitors.

ACKNOWLEDGEMENT
This work is funded by the NSFC (No.51869002), Jiangxi New Energy Technology and Equipment Engineering Technology Research Center (JXNE2016-09), the Fundamental Science on Radioactive Geology and Exploration Technology Laboratory (No. RGET1811), and the Innovation Fund Designated for Graduate Students of East China University of Technology (DHYC-201914).

References

1. Y. Qian, C.Y. Wang, F.L. Gao, *Biosens. Bioelectron.,* 63 (2015) 425.
2. Y. Qian**,** C.Y. Wang, F.L. Gao, *Talanta,* 130 (2014)33.
3. Y. Qian, D.Q. Tang, L.L. Du, Y.Z. Zhang, L.X. Zhang, F.L. Gao, *Biosens. Bioelectron.,* 64 (2015) 177.
4. Y. Qian, F.L. Gao, L.L. Du, Y. Zhang, D.Q. Tang, D.Z. Yang, *Biosens. Bioelectron.*,74 (2015) 483–490.
5. F.L. Gao, Y. Qian, L. Zhang, S.Z. Dai, Y.F. Lan, Y. Zhang, L.L. Du, D.Q. Tang, *Biosenors. Bioelectron.,* 71(2015) 158.
6. Y. Qian, T.T. Fan, P. Wang, X. Zhang, J.J. Luo, F.Y. Zhou,Y. Yao, X.J. Liao,Y.H. Li, F.L. Gao, *Sensor. Actuat. B,* 248 (2017) 187.
7. Y. Qian, C.L. Huang, R. Chen, S.Z. Dai, C.Y. Wang., *Int. J. Electrochem. Sci.*, 11 (2016) 7453.
8. T. Zhu, J.B. Ding, Q. Shao, Y. Qian, X.Q. Huang, *ChemCatChem.,* 11(2019)689.
9. M.W. Zhu, Q. Shao, Y.C. Pi, J. Guo, B. Huang, Y. Qian, X.Q. Huang, *Small*,13 (2017) 1701295.
10. T. Qi, J. Jiang, C. Chen, H. Wan, L. Miao, L. Zhang, *Electrochim. Acta,* 114(2013)674.
11. S. Chen, J. Zhu, X. Wu, Q. Han, X. Wang,*ACS nano*, 4 (2010)2822.
12. J. Bae, M.K. Song, Y.J. Park, J.M. Kim, M. Liu, Z.L. Wang, *Angew. Chem. Int. Edit.*, 50 (2011) 1683.
13. Z. Chen, Y. Qin, D. Weng, Q. Xiao, Y. Y. Peng, X. Wang, H. Li, F. Wei, Y. Lu, *Adv. Funct. Mater.,*19 (2009) 3420.

14. C. Zhao, X. Shao, Y. Zhang, X. Qian, *ACS Appl. Mater. Interfaces*,8(2016) 30133.
15. Q. Qu, S. Yang, X. Feng, *Adv. Mater.,*23 (2011) 5574.
16. Y. Wang, Y. Xia, *Adv. Mater.*, 25 (2013) 5336.
17. J. Xiao, S.Yang,*ChemPlusChem*, 77 (2012) 807.
18. J. Huang, Y. Xiao, Z. Peng, Y. Xu, L. Li, L. Tan, K. Yuan, Y. Chen, *Adv. Sci.*, 6 (2019) 1900107.
19. Z.-H. Huang, Y. Song, D.-Y. Feng, Z. Sun, X. Sun, X.-X. Liu, *ACS nano*,12 (2018) 3557.
20. B. Huang, C.L. Huang, Y. Qian, *Int. J. Electrochem. Sci.*, 12 (2017) 11180.
21. D. Zheng, H. Feng, X. Zhang, X. He, M. Yu, X. Lu, Y. Tong, *Chem. Commun.*,53 (2017) 3929.
22. J. Zhu, L. Cao, Y. Wu, Y. Gong, Z. Liu, H.E. Hoster, Y. Zhang, S. Zhang, S. Yang, Q. Yan, *Nano let.*, 13 (2013) 5408.
23. J.F. Chen, T. Zhu, X.P. Fu, G.Y. Ren, C.Y. Wang, *Int. J. Electrochem. Sci,* 14 (2019) 7302.
24. Z. Ma, X. Huang, S. Dou, J. Wu, S. Wang, *J. Phys. Chem. C*, 118 (2014) 17231.
25. Y. Bu, S. Wang, H. Jin, W. Zhang, J. Lin, J. Wang, J. Electrochem. Soc.,159(2012) A990.
26. S. Mondal, U. Rana, S. Malik, *J.Phys. Chem. C*, 121 (2017) 7573.
27. X. Yang, F. Zhang, L. Zhang, T. Zhang, Y. Huang, Y. Chen, *Adv. Funct. Mater.*, 23 (2013) 3353.
28. V. Nithya, N. Arul, *J. Mater. Chem. A***,** 4 (2016) 10767.
29. X. Zhao, C. Johnston, A. Crossley, P.S. Grant, *J. Mater. Chem.*, 20 (2010) 7637.
30. H. Xu, B.W. Zeiger, K.S. Suslick, *Chem. Soc. Rev.*, 42 (2013) 2555.
31. E. Mitche, R.K. Gupta, K. Mensah-Darkwa, D. Kumar, B.K. Ramasamy, B.K. Gupta, P. Kahol,*New J. Chem.*, 38 (2014) 4344.
32. W.-H. Khoh, J.-D. Hong, *Colloid. Surface. A*, 436(2013) 112.
33. W. Meng, W. Chen, L. Zhao, Y. Huang, M. Zhu, Y. Huang, Y. Fu, F. Geng, J. Yu, X. Chen, *Nano Energy*, 8(2014) 140.
34. S. Ghasemi, F. Ahmadi, *J. of Power Sources*, 289(2015)129.
35. C.Yi,J.Zou, H. Yang, X. Leng, *New J. Chem.*, 42 (2018) 7066.
36. A.K.Das,S.Sahoo,P.Arunachalam,S.Zhang, J.-J.Shim, RSC Adv., 6(2016) 107057.
37. Y. Qian, I.M. Ismail, A. Stein, *Carbon,* 68(2014)221.
38. M. Wang, X. Duan, Y. Xu, X. Duan, *Acs Nano*, 10 (2016) 7231.
39. J. Duan, Y. Zheng, S. Chen, Y. Tang, M. Jaroniec, S. Qiao, *Chem. Commun.*, 49 (2013) 7705.
40. Y. Qian, F. Ye, J. Xu, *Int. J. Electrochem. Sci.*, 7 (2012) 10063-10073.
41. Z. Qiang, Y. Xia, X. Xia, B.D. Vogt, Chem. Mater., 29 (2017) 10178-10186.
42. H. Chen, Y. Xiong, T. Yu, P. Zhu, X. Yan, Z. Wang, S. Guan, *Carbon*, 113 (2016)266-273.
43. L. Li, P. Gao, S. Gai, F. He, Y. Chen, M. Zhang, P. Yang, Electrochim. Acta, 190 (2016) 566-573.
44. D. Guan, Z. Gao, W. Yang, J. Wang, Y. Yuan, B. Wang, M. Zhang, L. Liu, *Mater. Sci. Eng.B,*178 (2013) 736.
45. Q. Wang, L. Jiao, H. Du, Y. Wang, H. Yuan, *J. Power Sources*, 245(2014)101.
46. C.-H. Xu, P.-Y. Shen, Y.-F. Chiu, P.-W Yeh, C.-C. Chen, L.-C. Chen, C.-C. Hsu, C.-C Cheng, J.-Z. Chen, *J. Alloys Compd,*676(2016), 469.
47. D. Liu, X. Wang, X. Wang, W. Tian, J. Liu, C. Zhi, D. He, Y. Bando, D. Golberg, *J. Mater. Chem. A*, 1 (2013) 1952.
48. J. Mu, B. Chen, Z. Guo, M. Zhang, Z. Zhang, P. Zhang, C. Shao, Y. Liu, *Nanoscale*, 3 (2011) 5034.
49. C. Fu, A. Mahadevegowda, P. Grant, *J. Mater. Chem. A*, 3 (2015)14245-14253.